Supporting Information: Simultaneous deep tunneling and classical hopping for hydrogen diffusion on metals

Wei Fang,[1] Jeremy O. Richardson,[2,*] Ji Chen,[3] Xin-Zheng Li,[4,†] and Angelos Michaelides[3,‡]

[1] *Thomas Young Centre, London Centre for Nanotechnology and Department of Chemistry, University College London, London WC1E 6BT, UK*

[2] *Laboratory of Physical Chemistry, ETH Zurich, CH-8093 Zurich, Switzerland*

[3] *Thomas Young Centre, London Centre for Nanotechnology and Department of Physics and Astronomy, University College London, London WC1E 6BT, UK*

[4] *School of Physics and the Collaborative Innovation Center of Quantum Matters, Peking University, Beijing 100871, P. R. China*

OUTLINE

Here we provide more computational details of the simulations reported in the manuscript and additional discussions in support of the conclusions reached. The tests on the computational setup and validity for our density functional theory (DFT) diffusion barriers are given in section S.I. The transmission action of all the barriers calculated and the Eckart barrier are discussed in section S.II. In section S.III we provide details about the model potentials we used for comparing quantum rate theories, and show further details and results of our RPMD simulations. We discussion the effects of dimensionality in section S.IV. In section S.V we provide more details for the new definition of classical to quantum transition temperature. In section S.VI isotope effects are discussed. In section S.VII we show the discussions on the existing experiments on Pt(111).

S.I. COMPUTATIONAL SETUP FOR THE DFT CALCULATIONS

For the transition metals we have considered, DFT correctly predicts the lattice constants and the H adsorption site on each surface examined. The vibrational frequencies computed are also in good agreement with experiments available. For example on Pd(110), electron-energy-loss spectroscopy (EELS) measured two clear peaks at 96-100 and 121-122 meV for hydrogen (and $\sim 1/\sqrt{2}$ of the two values for deuterium) [1]. Our frequency calculations show that they agree spot on with the outer plane vibration at the long bridge site (98 meV) and the pseudo-three-fold hollow site (120 meV). Our calculations on Ni surfaces reproduces experimental adsorption energies reasonably well [2, 3] and agreed very well with previous DFT studies [4].

To obtain reliable H diffusion barriers, the precise DFT setup for each system was determined after a careful set of tests. We examined the convergence of the adsorption energy:

$$E_{\rm ad} = E_{\rm H+surf} - E_{\rm surf} - 1/2E_{\rm H_2}, \tag{S1}$$

with respect to the plane wave energy cutoff, K-points, and number of layers in our DFT calculations on the high symmetry adsorption sites on the various surfaces discussed in the manuscript. We also examined the convergence of the relative energy difference between the high symmetry sites on the surfaces. The top two layers of surface atoms are flexible in our calculations.

metal	En-cut (eV)	K-points	unit cell	N layers	E_{ad} 3H	E_{ad} SB	ΔE (eV)
Pd	**350**	**4×4×1**	**2×3**	**7**	-0.525	-0.445	0.080
	350	4×4×1	2×3	8	-0.512	-0.410	0.102
	350	6×6×1	2×3	8	-0.503	-0.405	0.098
	350	4×4×1	2×3	10	-0.523	-0.435	0.088
Ni	**400**	**4×4×1**	**2×3**	**8**	-0.432	-0.368	0.064
	500	4×4×1	2×3	8	-0.434	-0.370	0.064
	400	6×6×1	2×3	8	-0.429	-0.364	0.065
	400	4×4×1	2×3	10	-0.442	-0.376	0.066

TABLE S1. Convergence of the plane wave energy cutoff, K-points, and number of layers for the DFT calculations on the (110) surface of Pd and Ni. The E_{ad} (units in eV) of the pseudo-3-fold hollow site (3H) and the short bridge site (SB) are compared, and ΔE is the energy difference between the two sites. The parameters used in the NEB calculations are given in bold.

metal	En-cut (eV)	K-points	unit cell	N layers	E_{ad} H	E_{ad} B	ΔE (eV)
Ni	**400**	**5×5×1**	**2×2**	**8**	-0.523	-0.426	0.097
	500	8×8×1	2×2	10	-0.510	-0.405	0.105
Cu	**400**	**7×7×1**	**2×2**	**8**	-0.177	-0.065	0.112
	500	9×9×1	2×2	10	-0.138	-0.048	0.090

TABLE S2. Convergence of the plane wave energy cutoff, K-points, and number of layers for the DFT calculations on the (100) surface of Ni and Cu. The E_{ad} of the hollow site (H) and the bridge site (B) are compared, and ΔE is the energy difference between the two sites. The parameters used in the NEB calculations are given in bold.

The test results are given in Table S1 ((110) surface), Table S2 ((100) surface), and Table S3 ((111) surface). We used a tight force convergence criterion (0.002 eV/Å) in our geometry optimisation and nudged elastic band (NEB) calculations [5]. The parameters used for the NEB calculations in the manuscript are given in bold, which converge the relative energies of the adsorption sites to within 20 meV.

We also tested the impact of different exchange-correlation functionals on the diffusion barriers. To this end, we have performed NEB calculations with the PBE-D3 and

metal	En-cut (eV)	K-points	unit cell	N layers	E_{ad} FCC	E_{ad} HCP	ΔE (eV)
Ni	**400**	**5×5×1**	**2×2**	**8**	-0.581	-0.568	0.013
	500	7×7×1	2×2	10	-0.552	-0.542	0.010
Cu	**400**	**7×7×1**	**2×2**	**8**	-0.189	-0.175	0.014
	500	9×9×1	2×2	10	-0.207	-0.192	0.015
Pd	350	4×4×1	2×2	7	-0.567	-0.525	0.042
	350	**6×6×1**	**2×2**	**8**	-0.583	-0.550	0.033
Pt	**400**	**5×5×1**	**2×2**	**8**	-0.485	-0.445	0.040
	400	9×9×1	2×2	8	-0.501	-0.462	0.039
	500	9×9×1	2×2	10	-0.487	-0.450	0.037

TABLE S3. Convergence of the plane wave energy cutoff, K-points, and number of layers for the DFT calculations on the (111) surface of Ni, Cu and Pt. The E_{ad} of the FCC site and HCP site are compared, and ΔE is the energy difference between the two sites. The parameters used in the NEB calculations are given in bold.

optB88-vdW functional for both a broad-top example (Ni(100)) and a parabolic-top example (Pd(111)). These two functionals incorporate dispersion interactions, which are not captured with the PBE functional that was used throughout this study. The results are shown in Fig. S1(a). Overall we have not found any example where a change in functional led to a qualitative change in the nature of the diffusion profile. Different functionals, as expected, yield slightly different energy barriers but in all cases the broad top barriers remain broad topped and the parabolic barriers remain parabolic.

We also considered the zero point energy (ZPE) of the H diffusion barriers. Two examples, Cu(100) and Ni(100), are shown in Fig. S1(b), one can see that the shape of the barriers changed little. ZPE increased the barrier height, this is because the transition states have more higher-frequency vibrational modes than the initial state.

S.II. TRANSMISSION ACTION OF THE DFT BARRIERS

The exact transmission probability $P(E)$ for H crossing a 1D barrier as a function of the incident energy E can be calculated by solving the time-independent Schrödinger equa-

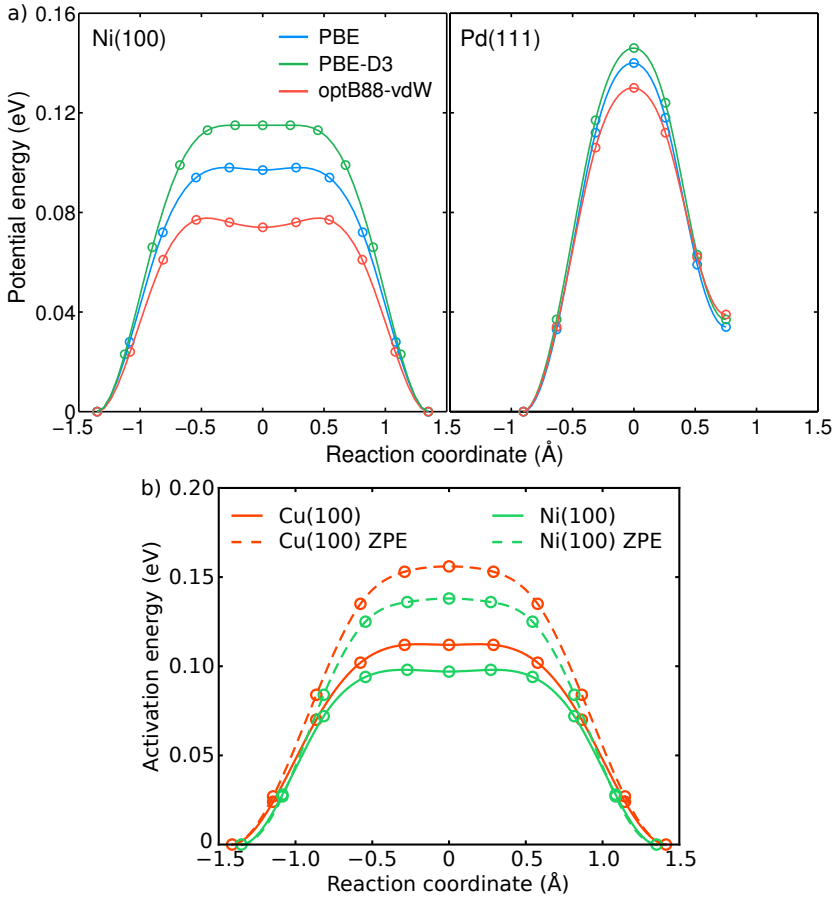

FIG. S1. (a) Comparison of the effect of functionals on the H diffusion barriers. The points are obtained from NEB calculations. (b) Comparison of the impact of ZPE of H on the barrier shape.

tion numerically using the Numerov method. $P(E)$ is the key quantity for quantum rate calculations. Integrating the thermal transmission probability $P(E)e^{-\beta E}$ gives the thermal diffusion rate at temperature T:

$$kZ_{\mathrm{r}} = \frac{1}{2\pi\hbar}\int_0^\infty P(E)e^{-\beta E}dE, \tag{S2}$$

where $\beta = \frac{1}{k_{\mathrm{B}}T}$, k_{B} is the Boltzmann constant and the scattering partition function $Z_{\mathrm{r}} = \sqrt{\frac{m}{2\pi\beta\hbar^2}}$, m is the mass of H, is used for the 1D barriers. The transmission action (defined as $-\hbar\ln(P)$) of all the barriers in Fig. 1 of the main text are shown in Fig. S2. The broad-top barriers (Ni(100), Ni(110) and Cu(100)) have a convex shape transmission action while the parabolic top barriers (Cu(111) and Pd(111)) have a concave shape transmission action. If the transmission action is exactly linear, at the transition temperature (Eq. S4), classical hopping, shallow tunneling and deep tunneling all contribute to the diffusion rate.

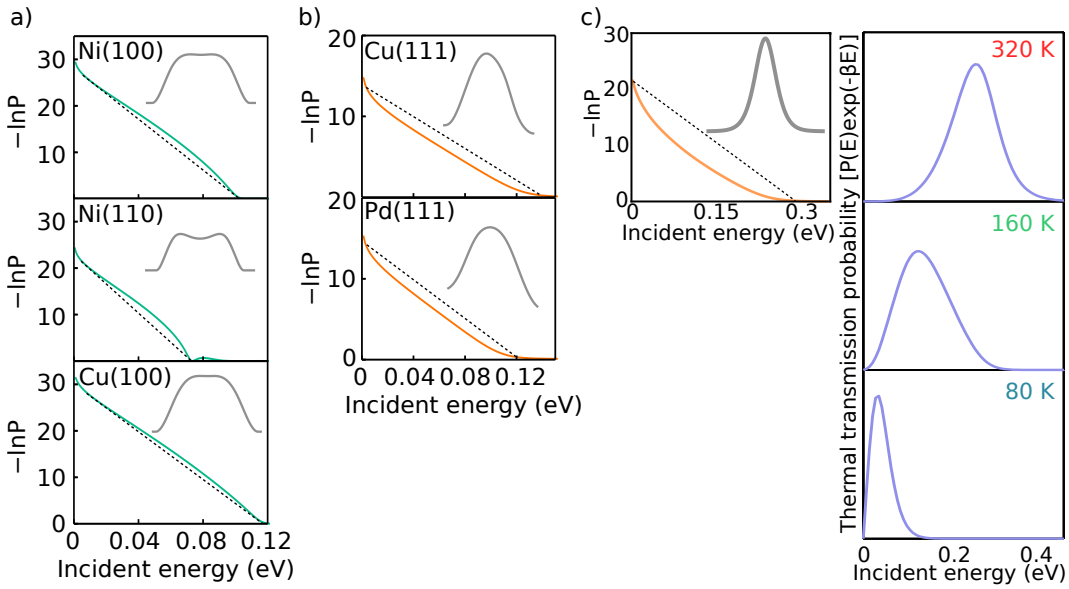

FIG. S2. a) The transmission action (in units of $\hbar$), as a function of the incident energy E for the broad-top barrier examples in Fig. 1 of the main text. They all have a convex shape. b) The exact transmission action of the parabolic-top barrier examples in Fig. 1 of the main text. They all have a concave shape. c) The exact transmission action of an Eckart barrier $V(x) = B\ \mathrm{sech}^2(x/a)$. The Eckart barrier parameters are the same as in [6], $a = 0.66a_0$, $B = \frac{72\hbar^2}{\pi^2 m a^2}$ ($\sim$0.25 eV), where a_0 is the Bohr radius and m is the mass of H, this barrier is $\sim$1 Å wide and the imaginary frequency at the top is ~ -1000 cm^{-1}. The thermal transmission probability plotted against the incident energy at three different temperatures are shown in the right panels.

S.III. COMPUTATIONAL DETAILS AND DISCUSSIONS FOR RPMD AND INSTANTON SIMULATIONS

We have tested the performance of different rate theories on a set of constructed barriers varying from cosine shape to broad-top shape with the functional form:

$$V(x) = E_{\mathrm{a}} \cos^2 \left[\left(\frac{2x}{w} \right)^{2r} \frac{\pi}{2} \right] \tag{S3}$$

in which $E_{\mathrm{a}} = 0.09$ eV, $w = 2.5$ Å, and $2r = 1,\ 3,\ 5$. $V = 0$ is used for $|x| > w/2$, as the abbreviated action in the instanton theory [7] and the WKB theory is independent of periodicity [8].

The ring polymer molecular dynamics (RPMD) rate [9], is calculated using the Bennett-Chandler method [10] that separates the rate into a dynamical factor multiplying a free

energy term [6, 11]. The free energy barriers were calculated using the potential of mean force method. 60 beads were used for the imaginary time path integral. The same number of beads was used for the instanton calculations, and the rates were converged with respect to the number of beads. A timestep of 0.5 fs was used and we ran a total of 20500 steps at each constrained centroid position, with the first 500 steps discarded for equilibration. With this simulation length, the average forces on the centroid of H have been converged to 10^{-3} eV/Å. The free energy barriers obtained are shown in Fig. S3. We see that on the broad-top barriers (2r=3 and 2r=5), the free energy barriers drop suddenly when the temperature decreases from 40 K to 30 K. The dynamical factor is calculated by performing thermostated-RPMD [12] simulations (with the friction factor $\lambda = 0.5$) starting with the ring polymer centroid at the barrier top (dividing surface). [13] The results are given in Table S4. We see that the RPMD dynamical factor is insignificant here as the centroid is a good dividing surface for a symmetric reaction, which is consistent with previous simulations [14].

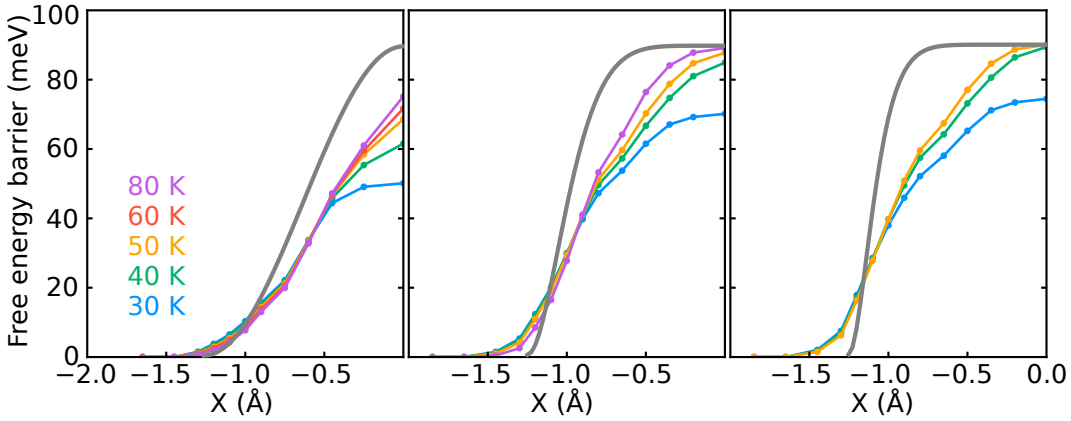

FIG. S3. Free energy barriers for the RPMD rate calculated with the potential of mean force method at different temperatures. The grey lines show the potential energy barriers (Eq. S3), with parameters $2r = 1$ (left), $2r = 3$ (middle) and $2r = 5$ (right).

Fig. S4 shows the comparison of different quantum rate theories on an even broader top barrier (Eq. S3, $2r = 5$) than the one discussed in the main text. The exact rate was computed using Eq. S2. We see more clearly that the conventional steepest-descent instanton (SDI) significantly underestimates the rate (by 2-3 orders of magnitude) and predicts the wrong transition temperature from classical hopping to quantum tunneling, because it fails to describe the physics of the process. SDI is numerically unstable below 35 K as the imaginary

Temperature (K)	2r=1 barrier	2r=3 barrier	2r=5 barrier
80	1.0	1.0	
60	1.0		
50	1.0	1.0	1.0
40	0.8	1.0	1.0
30	0.5	0.5	0.6

TABLE S4. The dynamical factor of the RPMD rate, rounded to one decimal.

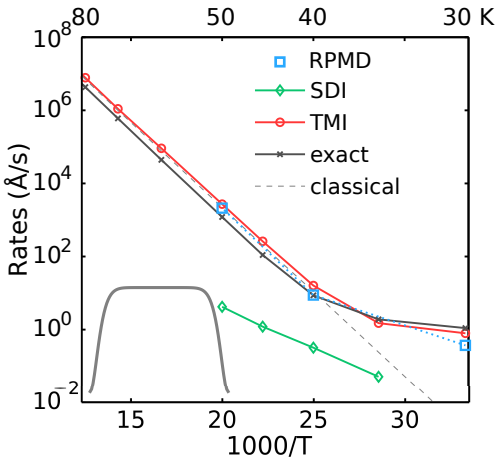

FIG. S4. Comparison of the diffusion rates on a broad-top barrier (Eq. S3) with parameter $2r = 5$, calculated using RPMD, steepest-descent instanton (SDI) [15], and the thermalized microcannonical instanton (TMI) [7] method.

frequency tends to 0. SDI is unable to accurately predict the rate at low temperature because the steepest-descent integration over energy is poor. As seen in Fig. 3c in the manuscript, the abbreviated action, W [7, 16], is approximately linear at low energies even though the $\mathrm{d}W/\mathrm{d}E$ must tend to $-\infty$ in this limit as the periodic orbit starting at $|x| = w/2$ has an infinite period. This implies a very strong contribution from higher derivatives of W which is therefore not well approximated by a second-order Taylor series and the steepest-descent integration. One could imagine generalizing the SDI to include both the low and high energy contributions, but this would not correct the errors in the rate at low T. On the other hand, both the RPMD and the recently developed thermalized microcannonical instanton (TMI) agree with the exact results well.

S.IV. 1D VS MULTI-DIMENSION

Here we discuss the effects of multi-dimensional treatment compared to 1D. First thing we considered is corner-cutting effects, which is interesting and can be important to the instanton path in many situations. For the diffusion paths we studied in this work, due to the fact that the H vibrational frequencies at the transition state perpendicular to the reaction coordinate are very stiff (> 1000 cm^{-1}) and the instanton has to satisfy symmetry requirements, it very difficult for the instanton path to deviate significantly from the minimal energy pathway. Hence we don't expect corner-cutting effects to be very important here. To show this we performed a full dimensional instanton optimization for the broad-top barrier on Pd(110) and compared the abbreviated action W to a 1D barrier with the same DFT setup (Fig. S5). It is clear that the W action barely changes going from 1D to multi-dimension. Because the W action is well-estimated by the 1D instanton, despite we do not expect our 1D calculations to give quantitative rate predictions, we do expect it to be able to predict the shape of the Arrhenius plot including the crossover temperature.

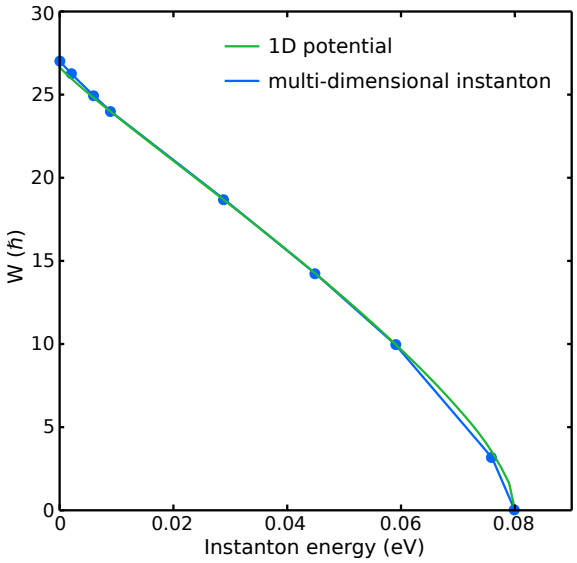

FIG. S5. Abbreviated action W versus instanton energy E for the 1D instanton and multi-dimensional instanton obtained on-the-fly with DFT for the short bridge H diffusion path on Pd(110).

Furthermore, we made comparison of 1D rates with full dimension rates and experimental rates. In our on going work, we have applied full dimensional TMI calculations to Pd(110)

surface. We found that the 1D rates can be reasonably good if the reactant and the transition state have similar zero point energies, which is the case for H diffusion over the short bridge path of Pd (110) (they differ by 6 meV). We also calculated 1D rates using a model barrier (Eq. S3, $2r = 2$) with experimental barrier height and width for Cu(100), which reasonably reproduced the STM experimental rates [17]. However we do not expect 1D rates to be always good and certainly do not want to promote using 1D model for accurate rate calculations.

Finally we consider effects of the surface atoms and heat bath. Previous path integral molecular dynamics studies [14, 18] have compared flexible and fixed surfaces for H diffusion on Ni(100) and the rates only change slightly. In addition, we have compared both a flexible and a fixed Cu(100) surface, where the barrier height is 112 meV and 118 meV for the flexible and fixed surface respectively. This also indicates that the movement of surface atom does not have a strong impact on the barrier. We also think including a heat-bath won't change our findings because the barrier top will always remain non-parabolic.

S.V. DISCUSSIONS ON THE TRANSITION TEMPERATURE FOR BROAD-TOP BARRIERS

In the manuscript, we have used the abbreviated action W to define an alternative transition temperature for the broad-top barrier:

$$T_W = \frac{\hbar}{k_\mathrm{B}} \frac{E_\mathrm{a}}{W_0}, \tag{S4}$$

where $W_0 = \oint \sqrt{2mV(x)}dx$ is the abbreviated action at incident energy $E = 0$. Here we show a simple derivation of an easy-to-apply equation of T_W for barriers with barrier height E_a and barrier width w:

$$
\begin{aligned}
T_W &= \frac{\hbar}{k_\mathrm{B}} \frac{E_\mathrm{a}}{W_0} \\
&= \frac{\hbar}{k_\mathrm{B}} \frac{E_\mathrm{a}}{2\int_{-w/2}^{w/2} \sqrt{2mV(x)}dx} \\
&= \frac{\hbar}{k_\mathrm{B}} \frac{E_\mathrm{a}}{2\sqrt{2mE_a}\frac{w}{2}\int_{-1}^{1} \sqrt{\frac{V(u)}{E_a}}du}, u = \frac{2x}{w} \\
&= \frac{\hbar}{n_s k_\mathrm{B}} \sqrt{\frac{E_\mathrm{a}}{2mw^2}} \\
n_s &= \int_{-1}^{1} \sqrt{\frac{V(u)}{E_a}} \mathrm{d}u \in (0, 2)
\end{aligned}
\tag{S5}
$$

n_s is a barrier shape factor that gives 2 for a square barrier and smaller values as the barrier becomes more curved.

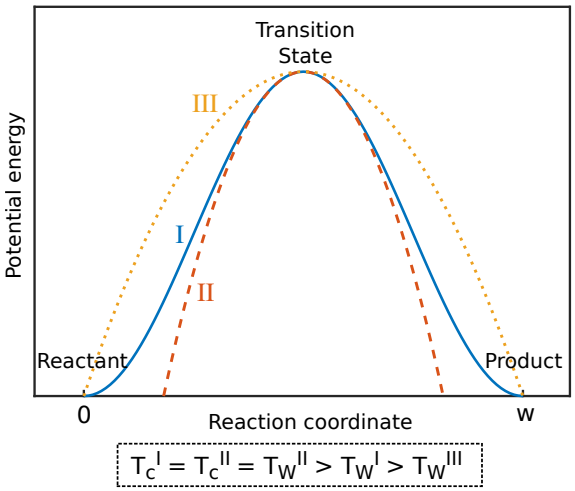

FIG. S6. Relations between T_c and T_W for a parabolic-top barrier. Barrier I is a parabolic-top barrier with width w and activation energy E_a. Barrier II is a parabola barrier with the same frequency at the transition state as barrier I. Barrier III is a parabola with width w and activation energy E_a. The T_c and T_W on these barriers follow the simple relation: $T_c^\mathrm{I} = T_c^\mathrm{II} = T_W^\mathrm{II} > T_W^\mathrm{I} > T_W^\mathrm{III}$.

Here we discuss the relation between the conventional crossover temperature $T_\mathrm{c} = \frac{\hbar\omega_b}{2\pi k_\mathrm{B}}$ and T_W for parabolic-top barriers. On a strict parabola $V(x) = E_\mathrm{a} - \frac{1}{2}m\omega_b^2 x^2$, the shape factor $n_s = \frac{\pi}{2}$, and the barrier width $w = \sqrt{\frac{8E_a}{m\omega_b^2}}$. Plugging into Eq. S5, one can find that for a strict parabola, $T_c = T_W$. Hence on parabolic-top barriers, the relation between T_c and

T_W is shown straightforwardly in Fig. S6. In summary, for broad-top barriers, T_W is well-defined and has a clear physical picture while T_c is not; on strict parabolas, $T_c = T_W$; and on parabolic-top barriers, both T_c and T_W are well-defined and closely related ($T_c > T_W$), but T_c has a clearer physical picture than T_W. The most suitable transition temperature for all barriers would ideally be given by combining T_c and T_W. For example, use the larger value between T_c^{I} and T_W^{I} (or T_W^{III}).

S.VI. ISOTOPE EFFECTS

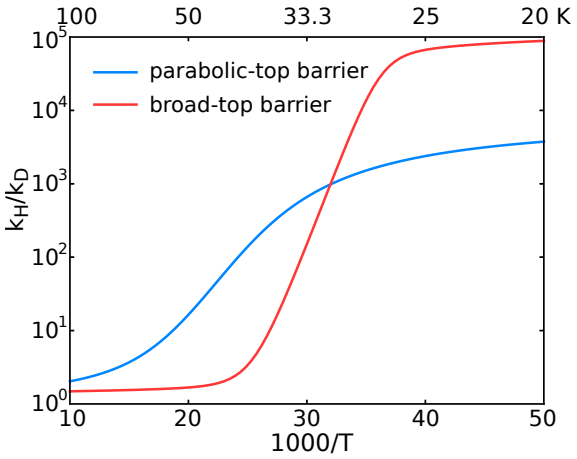

FIG. S7. Comparison of the H/D isotope effect, namely the diffusion rate ratio between H and D, on a broad-top barrier (Eq. S3, $2r = 3$) and on a conventional parabolic-top barrier (Eq. S3, $2r = 1$).

Fig. S7 shows a comparison of the H versus D diffusion rates, reported as $k_{\mathrm{H}}/k_{\mathrm{D}}$. Significant differences in the rates of H and D diffusion emerge rapidly within a narrow temperature window for broad-top barriers, whereas this happens much more gradually for parabolic-top barriers.

S.VII. MORE ON EXPERIMENTAL IMPLICATIONS

Fig. S8 shows our results on Pt(111). On this surface, HeSE [19] measured that the H diffusion rates is still temperature dependent even at 80 K and displays small quantum effects (only 1 order of magnitude higher than the classcial rate at 100 K), while LOD [20]

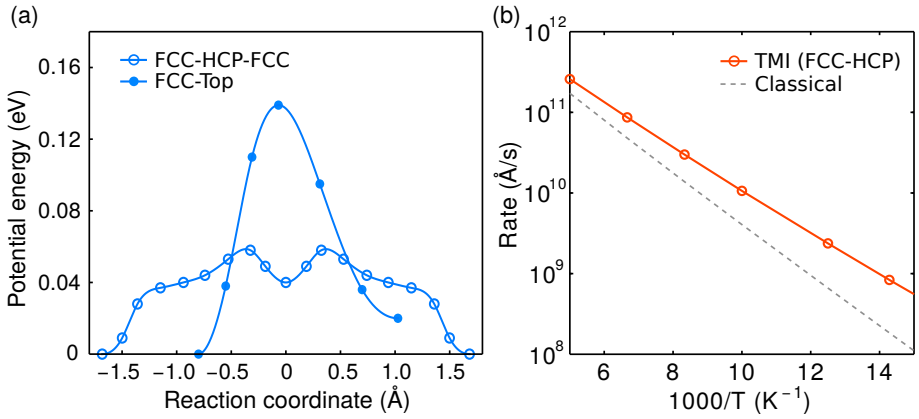

FIG. S8. (a) Potential energy barriers of H diffusion pathways on Pt(111). (b) The diffusion rate estimated using the TMI method for the FCC-HCP pathway in the temperature range 70 - 200 K.

experiment showed transition to temperature independent tunneling at 95 K. We calculated two diffusion pathways on this surface with NEB (Fig. S8(a)). The pathway FCC-Top has a much higher energy barrier than the pathway from FCC-HCP and hence is not expected to contribute much at these temperatures. The pathway FCC-HCP has an energy difference of 40 meV between the FCC and HCP sites and there is a small barrier at the bridge. Only shallow tunneling from FCC to HCP can happen and the rate should be temperature dependent down to very low temperatures when deep tunneling from FCC to another FCC occurs or deep tunneling between the FCC and top site becomes competitive. The rates calculated on the DFT NEB barrier for Pd(111) also agree very well with the HeSE experiment rates (within a factor of 5). In this sense our results support the HeSE measurements.

* jeremy.richardson@phys.chem.ethz.ch

† xzli@pku.edu.cn

‡ angelos.michaelides@ucl.ac.uk

[1] N. Takagi, Y. Yasui, T. Takaoka, M. Sawada, H. Yanagita, T. Aruga, and M. Nishijima, Phys. Rev. B **53**, 13767 (1996).

[2] K. Christmann, R. J. Behm, G. Ertl, M. A. V. Hove, and W. H. Weinberg, J. Chem. Phys. **70**, 4168 (1979).

[3] J. Lapujoulade and K. Neil, Surf. Sci. **35**, 288 (1973).

[4] G. Kresse and J. Hafner, Surf. Sci. **459**, 287 (2000).

[5] G. Henkelman and H. Jónsson, J. Chem. Phys. **113**, 9978 (2000).

[6] G. A. Voth, D. Chandler, and W. H. Miller, J. Chem. Phys. **91**, 7749 (1989).

[7] J. O. Richardson, Faraday Discuss. **195**, 49 (2016).

[8] On a 1D periodic potential, coherent diffusion will happen and the rate is ill-defined.

[9] S. Habershon, D. E. Manolopoulos, T. E. Markland, and T. F. Miller, Annu. Rev. Phys. Chem. **64**, 387 (2013).

[10] D. Chandler, J. Chem. Phys. **68**, 2959 (1978).

[11] M. J. Gillan, Journal of Physics C: Solid State Physics **20**, 3621 (1987).

[12] M. Rossi, M. Ceriotti, and D. E. Manolopoulos, J. Chem. Phys. **140**, 234116 (2014).

[13] T. J. H. Hele and Y. V. Suleimanov, J. Chem. Phys. **143**, 074107 (2015).

[14] Y. V. Suleimanov, J. Phys. Chem. C **116**, 11141 (2012).

[15] J. O. Richardson, J. Chem. Phys. **144**, 114106 (2016).

[16] R. P. Bell, *Tunnel Effect in Chemistry* (Chapman & Hall, 1980).

[17] L. J. Lauhon and W. Ho, Phys. Rev. Lett. **85**, 4566 (2000).

[18] W. Wang and Y. Zhao, J. Chem. Phys. **130**, 114708 (2009).

[19] A. P. Jardine, E. Y. M. Lee, D. J. Ward, G. Alexandrowicz, H. Hedgeland, W. Allison, J. Ellis, and E. Pollak, Phys. Rev. Lett. **105**, 136101 (2010).

[20] C. Z. Zheng, C. K. Yeung, M. M. T. Loy, and X. Xiao, Phys. Rev. Lett. **97**, 166101 (2006).